# Chapter 5

## 5.1 Introduction

Organic thin-film transistors, also known as OTFTs, offer many advantages over their inorganic materials, including lower production costs and more flexibility. First, the organic semiconductors (OSCs) and polymer gate dielectric stack with decreased temperature and quick thermal treatment practices are consistent with good output printing-based manufacturing [337] and also offer significant inherent material flexibility [338,339], or even expandability [340,341] for truly flexible and expandable electronics. Second, OSCs have a lot of potential for continual improvement and chemical modification via molecule structure crafting [342,343], and physical mingling [344], which opens the doors for enhancing product quality or distinguishing products by modifying the active materials rather than the manufacturing operations. In conclusion, by engaging non-flat panels with flexible displays, sensors, and other electronic functionalities, the OTFT approach can deliver electrical, mechanical, and commercial benefits to a variety of applications. Encouraged by these, major investigations in OTFT technologies, including materials, processes, devices, circuit assembly, and applications, have been made in recent decades, resulting in tremendous advancements [345]. Various researchers and corporations have also reported a slew of noteworthy advancements in device manufacturing, circuit assembly, and OTFT applications [346-350].

In this context, semiconducting polythiophene materials such as poly(3-hexylthiophene) (P3HT), Poly[5,5′-bis(3-dodecyl-2-thienyl)-2,2′-bithiophene] (PQT), and Poly(2,5-bis(3-alkylthiophen-2-yl)thieno[3,2-b]thiophene) (PBTTT) are intriguing materials due to their relatively high mobility combined with solution processibility, enabling large area electronics and optoelectronics on pliable substrates at minimal expense. A higher degree of structural ordering is projected to improve carrier delocalization, which will result in increased mobility [351,352]. It has been shown that poly(2,5-bis(3-alkylthiophene-2-yl)thieno[3,2-b]thiophenes) (pBTTT) exhibits hole mobility that is similar to what is achievable with amorphous silicon and is comparable to the charge carrier mobility of several small molecule semiconductors. This value might be connected to the improved crystallinity found in PBTTT thin films, which contain domains made up of alkyl-stacked lamellar and π-π stacked polymer chains. Carbon-

based nanofillers have been extensively used in the fabrication of nanocomposites with polymer framework to convey their good mechanical strength and rigidity, as well as their excellent thermal and electrical conductivity, to the bulk system. Because of its outstanding optical, thermal, and mechanical capabilities, graphene has earned a special place among carbon nanomaterials [259,353,44,354]. Graphene is a two-dimensional structure made up of a single layer of carbon atoms having $sp^2$ hybridisation [355]. Owing to its zero band gap, pure graphene has limited electrical and optical applications [44,356]. In this regard, Graphene quantum dots (GQDs) are graphene sheets with a few layers stacked on top of each other that have lately emerged as new carbon-based materials [357]. GQDs, which combine the benefits of graphene and quantum dots, have been recognised as an emergent nano-material and used in a variety of applications, including bio-imaging [354], catalyst [358], energy [359], sensing [360] and optoelectronic devices [361] and so forth. Because GQDs include a large number of chemical moieties, such as epoxy and hydroxyl groups on the basal plane and carboxyl groups on the edges, they have a high water solubility and may be functionally modified in a variety of ways [362]. Nanoparticles have made it possible to manipulate the features of polymer frameworks. The demand for the controlled production of long-lasting graphene-based electrically conductive polymer composites is what is igniting interest in conductive GQDs composites. Therefore, the properties of the polymer matrix, such as low density and flexibility, can be integrated with the mechanical or other physical qualities of the filler by incorporating a filler into the polymer framework. The interface between the polymer framework and nanofiller, which impacts the uniformity of dispersion and amount of the filler, is one of the most important elements determining the functionality of nanocomposites [363]. This has been overcome by introducing graphene nanoparticles into the polymer via chemical alteration, either covalent or noncovalent [364,365].

It is the crystallinity of these π-conjugated polymers in the bulk and on the interfaces that is essential for effective device performance [366,367]. The crystallinity of thin films may be increased using a variety of polymer film deposition procedures, including spin-coating (SC), friction transfer (FT), drop casting (DC), floating film transfer method (FTM), and others [368-371]. The traditional spin coating technique is said to produce isotropic thin films that are arbitrarily ordered and curled. Thin films produced from the FTM, on the other side, are extremely crystalline with increased grain size, as

evidenced by the group's earlier AFM studies [372-376]. Spin-coated films have already been shown to be amorphous, whereas FTM films have more organised domains [374]. Therefore, using the FTM technique not only improves device efficiency for the films prepared by FTM [374,377] but it can also be used to achieve molecular orientation of conducting polymers with useful applications in eolotropic optoelectronics [378-380].

In this report, we have synthesized graphene quantum dots(GQDs) from graphite by chemical oxidation. GQDs were transported from an aqueous solution to chloroform through ultrasonication before the production of the PBTTT/GQDs nanocomposite. For the production of the PBTTT/GQDs solution, chloroform-dispersed GQDs were used. Afterwards, PBTTT/GQDs nanocomposite is formed by sonication and stirring and 15 µl of this solution is dropped and cast on ethylene glycol: glycerol (1:1) to form a floating film. The morphological, structural, spectroscopic, and electrochemical characteristics of an as-deposited polymer film were evaluated and contrasted with those of a virgin polymer film. The polymer nanocomposite film was used to make thin film transistors, which demonstrated better device performance under ambient conditions

## 5.2 Results and Discussion

### 5.2.1 Characterization of Graphene quantum dots(GQDs)

The optical characteristics of GQDs were studied using UV-vis and PL techniques. The UV–vis absorption spectrum of the GQDs aqueous medium is shown in Fig. 5.1(a). The peak at 229 nm is allocated to the π-π* transition of $sp^2$ C=C aromatic domain while the band at 300 $cm^{-1}$ is allocated to the n-π* transition of C=O bonds present on the oxidized carbon surface. The inset of Fig.5.1(a) shows the green fluorescence of GQDs under UV light with 365 nm excitation. In Fig.5.1(b), the excitation relying on PL behaviours was observed in prepared GQDs. The emission wavelength changes when the excitation wavelength changes. The peak emission intensity decreases as the excitation wavelength increases. When excited from 300 to 525nm, the PL spectrum showed two peaks from excitation wavelength 300 to 400 nm. The PL peak showed only one peak as they were excited from 370 to 500 nm. The maximum PL intensity was achieved when the excitation wavelength was 350 nm. The optical range of variously sized GQDs, surface effects, differing emissive traps (salvation effect), or an

as-yet-unidentified mechanism has made the excitation-dependent PL behaviour of fluorescent carbon-based nanomaterials a hot topic [381]. Fig.5.1(c) shows the TEM image of GQDs where GQDs with diameters ranging from 2 to 10 nm and spherical are unanimously and densely concentrated in the products. The corresponding particle size distribution histogram (inset of Fig. 5.1c) shows that the average diameter of these dots is 3.7 nm. Fig.5.1(e) shows the FTIR absorption spectrum of GQDs having different functionalities attached due to the chemical oxidation of graphite. The -OH stretching and C-OH bending are responsible for the broad peaks at 3436 $cm^{-1}$ and 1375 $cm^{-1}$. There is a peak at 1632 $cm^{-1}$ that may be traced back to the C=C stretching vibration. Epoxy group(C-O-C), C-O bond absorption occurs at 1121 $cm^{-1}$ as well. At 1740 $cm^{-1}$, the carbonyl group has a C=O stretching vibration. To validate the chemical states and compositions of GQDs, XPS proved a useful technique. Fig.5.1(e) demonstrates the deconvolution of the C 1s band into four peaks, which correspond to the C=C, C-C, C-O (epoxy/alkoxy), and C=O(carbonyl and carboxylic) groups, respectively, at energies of 284.5 eV, 285.8 eV, 286.5 eV, and 287.9 eV.

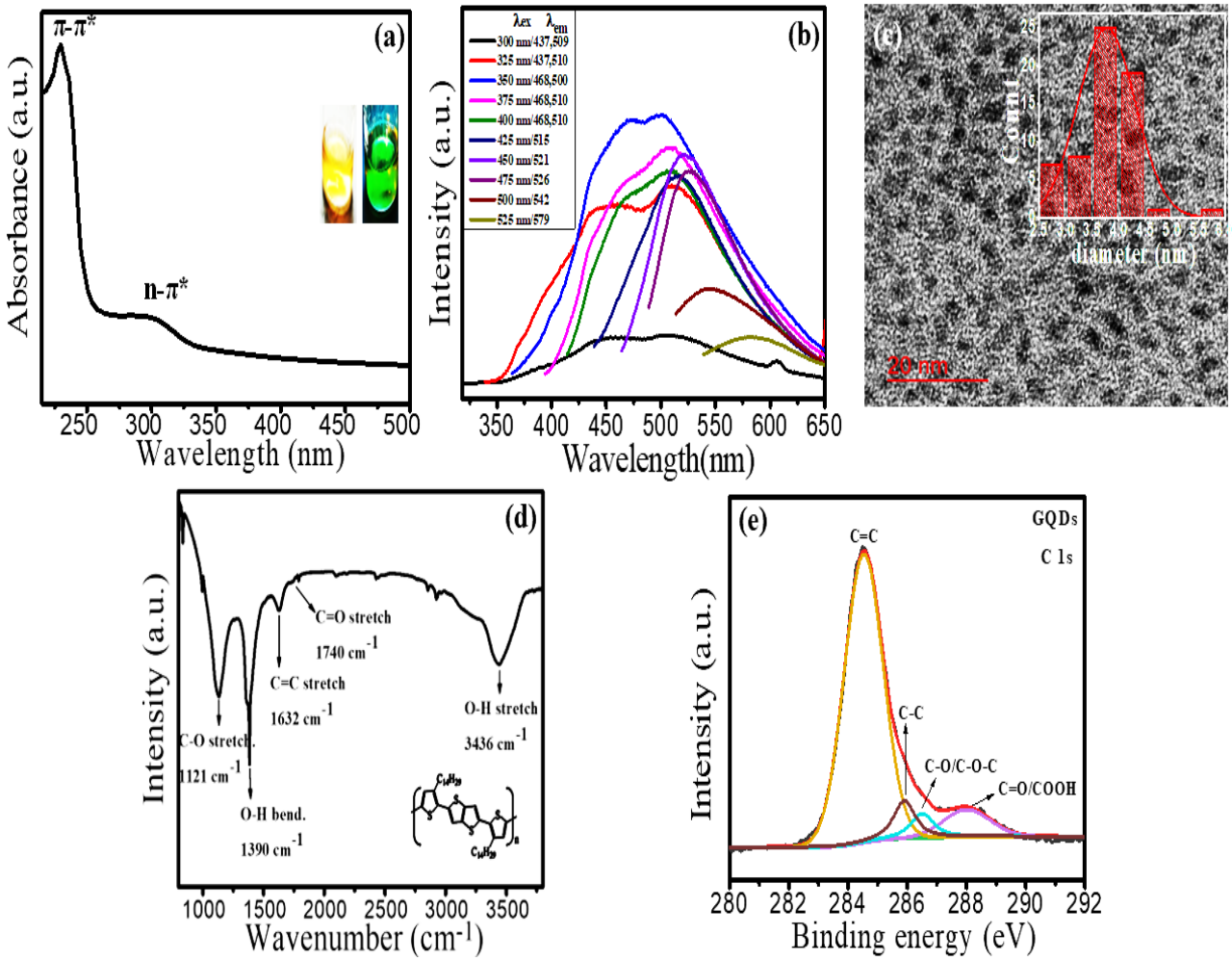


**Fig.5.1 (a) UV-Vis spectrum of GQDs,(b)Photoluminescence spectrum of GQDs,(c)TEM image of GQDs, where inset is showing corresponding particle size distribution histogram,(d)FTIR spectrum of GQDs,(e) XPS spectrum of C1s of GQDs.**

### 5.2.2 Characterization of PBTTT /GQDs nanocomposite film

XRD of all thin films lifted on glass substrates prepared by FTM is shown in Fig.5.2(a). The PBTTT/GQDs nanocomposite FTM film has two sets of reflections, (h00) for alkyl stacking of PBTTT chains and (0k0) for π-π stacking, with diffraction peaks numbered (100), (200), (300), (400), and (010) at 3.97°, 8.03°, 12.12°,16.61 and 24.31°, respectively. The diffraction peaks for (100), (200), (300), (400), and (010) in a pristine polymer film are 4.04°,8.32°,12.74°,16.95°, and 24.47°, respectively. The peak matching to diffraction planes (100),(200),(300), and (400) for the composite film has moved towards a lower angle compared to pristine film, resulting in a decrease in d-spacing. This modification might have occurred as a result of the charge transfer (CT) interaction between the filler and polymer. Peak intensity analysis of PBTTT/GQDs nanocomposite film reveals that the formed nanocomposite film produced using the FTM technique allows for the well-growth of polymer nanocomposite domains without thermal treatment. Although the peak intensity of the (100) diffraction peak is slightly lower than the pristine film, the peak intensity of the remaining peaks viz.(200),(300),(400) and (010) is increased than that of the pristine polymer film. It's worth mentioning that the (010) plane in the polymer is depicted by HR-TEM. However, powder XRD shows both (h00) and (0k0) reflections, with (h00) reflections having higher peak intensity than (0k0), indicating that the polymer film's shape is mostly edge-on. Fig. 5.2(b-d) shows a TEM image of a pure PBTTT and PBTTT/GQDs nanocomposite film over a Cu grid. Fig.5.2(b) shows the folded structure of the pristine polymer film, whereas the composite FTM film displays a regular deployment of GQDs in the PBTTT polymer matrix as seen in Fig.5.2(c,d). As a result, the TEM images clearly show the decoration of the GQDs into the PBTTT polymer framework. The picture of the composite film at a greater magnification may be seen in the inset of Fig.5.2(c). Only in the HR-TEM of the same sample is it possible to see the (010) plane, which corresponds to the π-π stacking (Fig. 5.2(d).In addition, the diffused rings in the SAED image of PBTTT/GQDs films (inset of Fig. 5.2(d)) provide evidence that the PBTTT/GQDs nanocomposite film has a polycrystalline structure.

A UV-Vis and FTIR absorption research was carried out and compared to a pristine sample to explore the interaction between PBTTT and GQDs, as depicted in Fig. 5.2 (e & f). The normalised electronic absorption of pure PBTTT films and PBTTT/GQDs

nanocomposite made by the FTM process is shown in Fig. 5.2 (e). These two types of films display high characteristic absorption at 541 and 553 nm, respectively, and right shoulder bands at 586 and 594 nm. The charge transfer (CT) relationship between polymer and GQDs is indicated by the expansion and increase of $\lambda_{max}$ of the band in PBTTT/GQDs nanocomposite films. This is in contrast to pure PBTTT films, which show no evidence of this interaction. As a result of interactions between molecules, the spectral response may move toward longer or shorter wavelengths in response to changes in the ratio of peak intensities ($A_{0\text{-}0}/A_{0\text{-}1}$) related to the simultaneous change in electronic and vibrational transition [287]. Because of this, as compared to the optical absorption of the pure PBTTT film, the UV-vis absorption spectra of the PBTTT/GQDs film exhibit a redshift, which demonstrates the participation of polymer-GQDs interaction. The amount of polymer aggregation indicating intermolecular interaction can be noticed in the absorption bands of thiophene thin films, according to the literature. Interchain and intrachain interactions caused by polymer chain aggregation can explain the red shift in absorption peaks. Planarization of the polymer backbone caused by aggregation causes red-shifting of optical transitions in these polymer aggregates [288,289,328]. As shown in Fig. 5.2(e), increasing the conjugation length and degree of polymer aggregation order increases the ratio of the lowest energy peak to the next replica peak. Because of the elevated peak ratio, the composite film has a greater degree of intrachain order, and as a consequence, a longer sequence of alternating single and double bond order. It has been shown in the scientific literature that GO or rGO may cause the formation of crystalline nanostructures in polymer chains [329,291,292]. Therefore, the longer conjugation distances in the presence of nano-sized GQDs sheets were the reason for the enhanced peak ratio ($A_{0\text{-}0}/A_{0\text{-}1}$) in PBTTT/GQDs composites.

Fig.5.2(f) depicts the various functionalities present in pure PBTTT and PBTTT/GQDs nanocomposite (b). The asymmetric C–H stretching vibrations observed in $–CH_3$, $–CH_2$ groups, and the symmetric C–H stretching vibrations present in $–CH_2$ in long alkyl chains of PBTTT polymer have been attributed to the peaks at 2972, 2926, and 2853 $cm^{-1}$, respectively. The bands at 1463, 1377, and 1410 $cm^{-1}$ are caused by thiophene ring C=C stretching, methyl and methylene deformation of the alkyl chain. The C-S in-plane stretching vibration has a frequency of 816 $cm^{-1}$. The C–H (in-plane) bending oscillations of the thiophene ring is thought to be responsible for the band that occurs at

1124 $cm^{-1}$. While the peak at 1780$cm^{-1}$ for the PBTTT/GQDS nanocomposite refers to C=O vibrations from carbonyl groups present in the GQDS. The wide peak at 1128 $cm^{-1}$ contains a minor shoulder peak at 1087 $cm^{-1}$, which may be ascribed to the C-O stretching vibration caused by the occurrence of epoxide groups in the GQDs nanosheet. This particular vibration is not evident in the pure polymer. In addition, when compared to pure PBTTT, the aromatic CH bending vibration in composite has increased intensity. This may be due to the O-H bending vibration present in GQDs broadening the peak around 1385 $cm^{-1}$. As a result, the FTIR results show character trait peaks in both components, indicating that GQDs were successfully incorporated into the PBTTT matrix. As a result, the FTIR results show character trait peaks in both components, implying that GQDs are successfully incorporated into the PBTTT matrix.

Moreover, as shown in Fig.5.2(g), Cyclic voltammetry measurements were used to investigate aggregation, charge transfer, and energy levels of the frontier orbitals of both films formed on the ITO substrate. PBTTT and PBTTT/GQDs nanocomposites have distinct differences in the overall appearance of oxidation peak positions. The lower one indicates the presence of aggregated PBTTT chains, whereas the higher one indicates the presence of both amorphous and aggregated PBTTT chains [331]. The HOMO level of both films was estimated to be -5.17 eV for the composite film and -5.29 eV for the pure polymer film by using the eqn. 5.1 from the observed onset oxidation potential. Similar findings were revealed by Istif et al., who said that the presence of GO stimulates the creation of polymer nanostructures in addition to the existence of charge transfer interactions, which ultimately leads to a reduction in the HOMO energy level [332]. Because of this, the changes that have occurred in the HOMO level and the characteristics of the absorption bands point to the fact that the composite material's electronic property has been altered. In the research that has been done so far, almost everyone has concluded that various morphologies have variable degrees of energy. In the scientific literature, it is widely agreed upon that various morphologies have varied energy levels and work functions of electrons. These differences are significant to morphology and electrical coupling between polymer chains [293,333]. CV is also connected to the work function of the material since it represents the movement of an electron from the highest energy level of a molecule (HOMO) to the material's surface. The oxidation peak obtained from the hybridization

of PBTTT with GQDs was entirely distinct from the one obtained from the pure compound.

$$E_{HOMO} = -e(4.4 + E_{ox(onset)})V \quad (5.1)$$

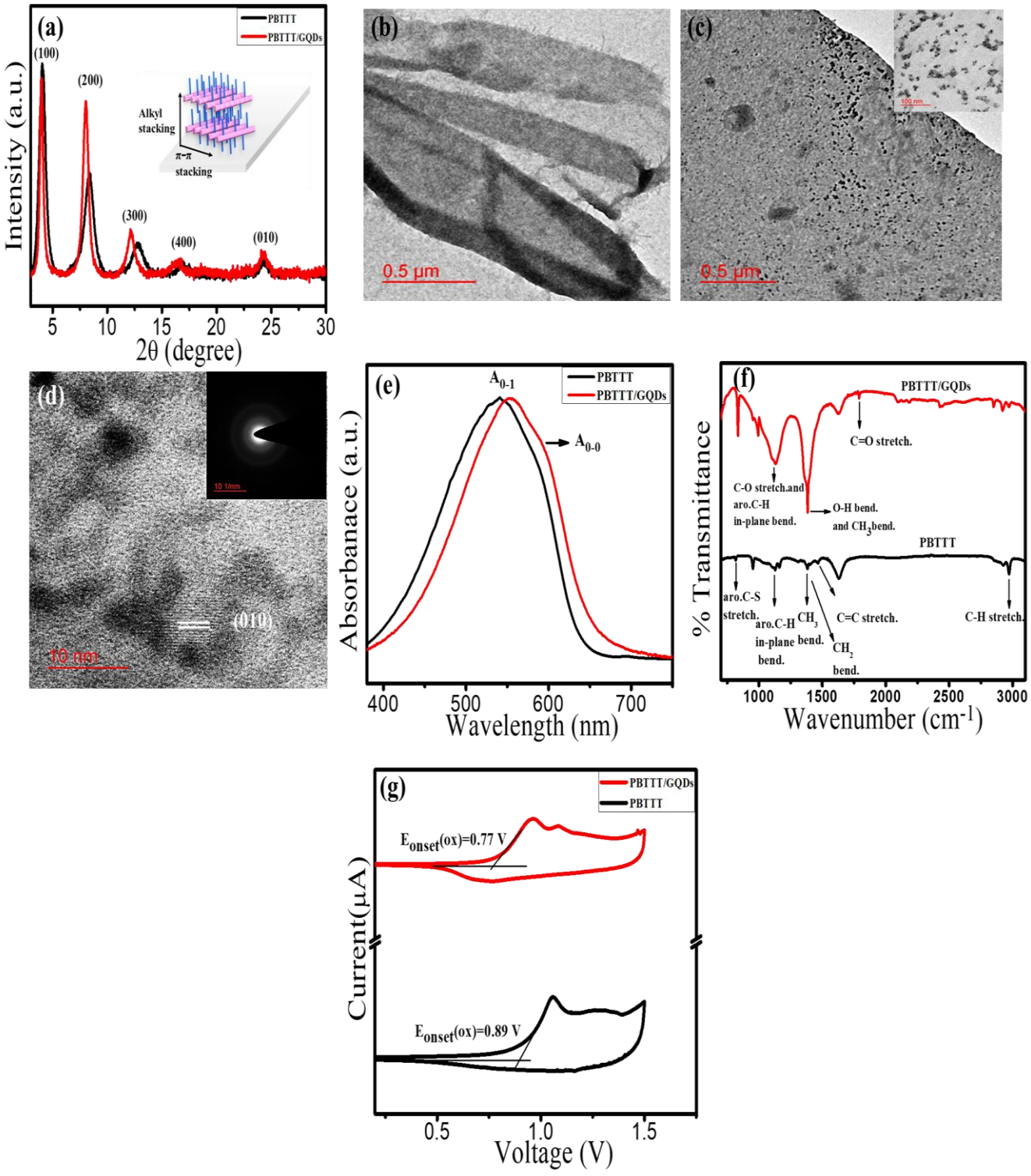


**Fig. 5.2 (a) Powder XRD of PBTTT and PBTTT/GQDs FTM film,(b) TEM image of PBTTT FTM film,(c) TEM image of PBTTT/GQDs FTM film, where inset shows the higher magnification image (d) HR-TEM image of composite film**

**showing (010) plane. The SAED picture of the PBTTT/GQDs FTM film is seen in the inset,(e) UV-Vis spectrum of PBTTT, and PBTTT/GQDs FTM film, (f) FTIR spectrum of PBTTT and PBTTT/GQDs (g) CV of PBTTT and PBTTT/GQDs FTM film over ITO coated glass substrate.**

### 5.2.3 Electrical Characterization

To investigate charge transport capabilities, 30 µm x 1 mm Au electrodes were placed on top. All chemistry, film deposition, device construction, and tests were done at room temperature and 55% relative humidity. Initial research demonstrates p-type $I_{DS}$-$V_{DS}$ output and $I_{DS}$-$V_{GS}$ transfer features. Fig.5.3(a,b) and (c,d) illustrates the output and transfer characteristics of pure polymer and nanocomposite film. In the saturated regime, the equation(5.2) calculated field effect mobility (µ) and on/off ratio from the transfer characteristics:

$$\boldsymbol{I_{DS} = \frac{W}{2L}\mu C_i(V_{GS} - V_{th})^2} \qquad \textbf{(5.2)}$$

Where, $I_{DS}$ stands for drain current, W and L for channel width and length, $C_i$ for capacitance per unit area, and $V_{GS}$ for gate voltage that is applied. Using the previously stated equation, the average mobility(µ) of PBTTT/GQDs film was calculated to be 0.16 $cm^2$/V.s at -40 V drain voltage, which is approximately 16 times that of pristine PBTTT film(µ=0.0095 $cm^2$/V.s) and more than 1.2 times in on/off ratio ($0.56x10^3$) under ambient conditions. The achieved low value of the on/off ratio can be explained by considering the measurement condition and concentration of GQDs nanosheets. All I-V measurements were carried out in open ambient settings with a relative humidity of 55 per cent, which led to a low on/off ratio. Additionally, the on-off ratio is lowered due to the incorporation of GQD nanosheets [274]. The procured value of high mobility can be validated by considering surface topography, GIXD, where PBTTT lamella are cohesively assisted by GQDs nanosheets. The surface micrograph verifies the

decorating of GQDs into the polymer PBTTT matrix, which creates a pathway that is well linked to the flow of charge carriers. HR-TEM images and XRD depict the formation of a highly edge-oriented self-assembled nanocomposite layer suitable for planner electronic gadgets. Thus, the co-operatively supported PBTTT lamella via GO improves crystallinity while also enabling charge transport, leading to an increase in composite output current and mobility [334]. Furthermore, the broadening of the polymer composite absorption band and maxima shift towards higher wavelength confirms the presence of charge transfer interaction between polymer and GQDs with lengthened intrachain order and molecule co-planarity. It is interesting to note that many forms of conduction paths are feasible in composite materials, suggesting the existence of percolative behaviour [335,336]. This percolation channel makes charge transfer easier because it lowers the resistance of the path that charge carriers take between the source electrode and the drain electrode. Changes in electrical characteristics, as well as shifts in the locations of HOMO and LUMO levels, are revealed whenever there is a shift in the oxidation potential. This HOMO level modification might increase charge carrier mobility in the semiconducting material while also improving the efficacy of charge carrier injection between electrodes and active materials [296].

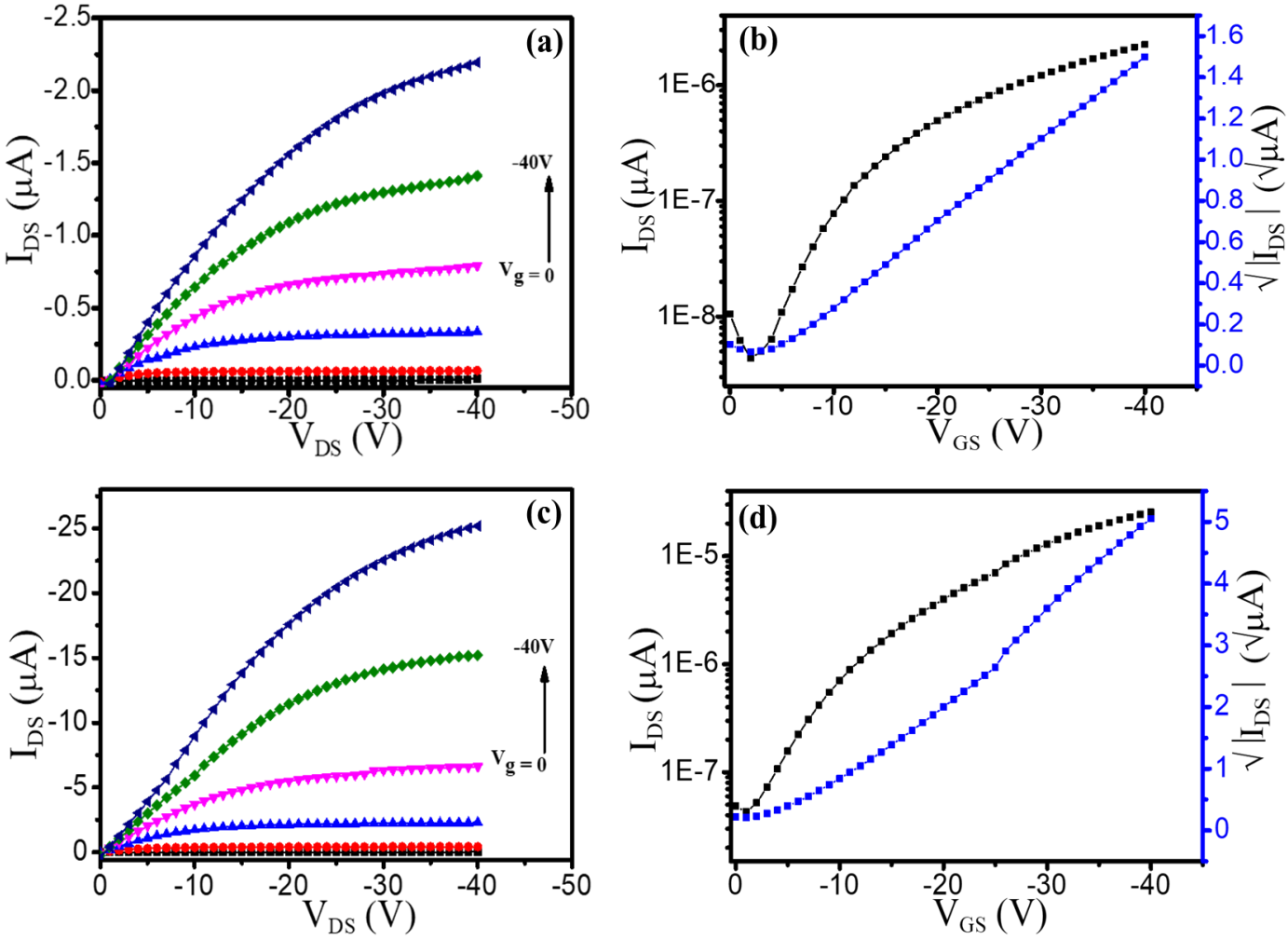


**Fig.5.3 Output ($I_{DS}$-$V_{DS}$) and transfer characteristics ($I_{DS}$-$V_{GS}$) of (a,b) pristine PBTTT and (c,d) PBTTT/GQDs nanocomposite FTM thin film**

A proper scattering of nanofillers in the polymer medium is critical to the OTFT's output. This resulted in a nearly similar curve with small current changes, as seen in Fig.5.5 when the film was captured from 10 different locations.

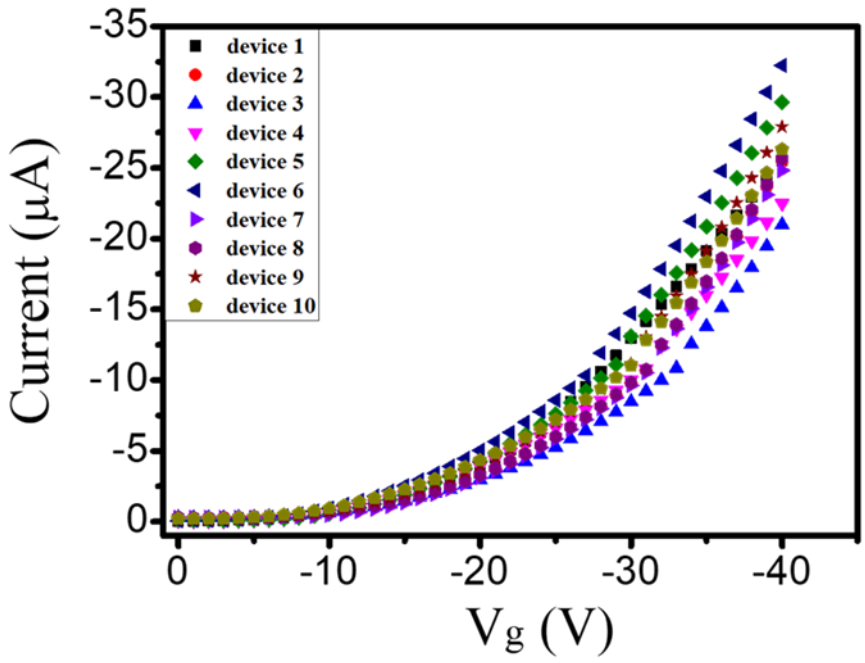


**Fig.5.4 $I_{DS}$-$V_{GS}$ transfer characteristics of PBTTT/GQDs nanocomposite thin film at 10 different places at $V_{DS}$= -40 V**

### 5.3.Conclusions

To develop solution-processable PBTTT/GQDs nanocomposites in chloroform, ultrasonication was performed. Furthermore, an FTM technique based on a liquid base with a high surface free energy was used to develop a simple method for producing self-assembled, highly oriented, anisotropic thin films of PBTTT /GQDs nanocomposites. The device fabrication is done by designing a top contact bottom gate structure having a gold metal electrode. The average field effect mobility(μ) of PBTTT/GQDs film is found to be 0.16 $cm^2$/V.s which is roughly more than 16 times that of pristine polymer (=0.0095 $cm^2$/V.s) and more than 2.8 times the on/off ratio of pristine polymer i.e. $0.56x10^3$ under ambient conditions. Thus, the PBTTT lamella co-supported by GQDs improves crystallinity while also enabling charge transport, increasing composite output current and mobility. By lowering the route resistance between the source and drain electrodes, this percolation path aids the conduction mechanism.